Elastic dipoles of point defects from atomistic simulations

Céline Varvenne*
Centre Interdisciplinaire des Nanosciences de Marseille, Aix-Marseille Univ.-CNRS, Campus de Luminy, F-13288 Marseille, France

Emmanuel Clouet
DEN-Service de Recherches de Métallurgie Physique, CEA, Université Paris-Saclay, F-91191 Gif-sur-Yvette, France
(Received 3 October 2017; published 19 December 2017)

The interaction of point defects with an external stress field or with other structural defects is usually well described within continuum elasticity by the elastic dipole approximation. Extraction of the elastic dipoles from atomistic simulations is therefore a fundamental step to connect an atomistic description of the defect with continuum models. This can be done either by a fitting of the point-defect displacement field, by a summation of the Kanzaki forces, or by a linking equation to the residual stress. We perform here a detailed comparison of these different available methods to extract elastic dipoles, and show that they all lead to the same values when the supercell of the atomistic simulations is large enough and when the anharmonic region around the point defect is correctly handled. But, for small simulation cells compatible with *ab initio* calculations, only the definition through the residual stress appears tractable. The approach is illustrated by considering various point defects (vacancy, self-interstitial, and hydrogen solute atom) in zirconium, using both empirical potentials and *ab initio* calculations.

DOI: 10.1103/PhysRevB.96.224103

I. INTRODUCTION

Point defects in crystalline solids, such as vacancies, self-interstitial atoms, solute atoms, or their small clusters, play a crucial role in controlling materials properties and their kinetic evolutions, particularly through their interaction with other defects, like dislocations, surfaces, interfaces, grain boundaries, and also other point defects. While *ab initio* calculations give an accurate description of such interactions at short range, this modeling approach is not tractable to characterize the long-range part because of the inherent size limitation of these simulations. For neutral defects, the long-range interaction is elastic and elasticity theory appears therefore as a natural modeling approach. A point defect can be described within elasticity theory through an equivalent distribution of point forces [1–3]. Of particular importance is the elastic dipole, a second-rank tensor which corresponds to the first moment of the force distribution, from which one can determine the long-range elastic field of the point defect and calculate its interaction with an external strain field. Extraction of this elastic dipole from atomistic simulations, in particular *ab initio* calculations, allows then to fully characterize and model the point defect within elasticity theory. This is essential for upscaling approaches, where mesoscale techniques are required to treat long-term evolutions and/or interactions of point defects with the complex elastic fields of various structural defects, and that must include the necessary information from the atomic scale. Accurate elastic dipole extractions thus allowed successful modeling of stress-driven diffusion [4,5] and more generally elastodiffusion [6,7], or of sink strength optimization of semicoherent interfaces [8]. Furthermore, their extraction enables to set up finite-size correction schemes to obtain the energy of an isolated point defect from *ab initio* calculations relying on periodic boundary conditions [9]. However, because of the small size of *ab initio* simulations, computation of such accurate values of elastic dipoles may be challenging.

There is a rather long history of extraction of elastic dipoles from atomistic simulations, mainly using empirical potentials. The Kanzaki method [1,10], based on the measurement of the defect-induced forces, has been widely used for vacancies in ionic crystals and various point defects in metals [11–16]. This approach relies on the harmonic approximation, which has been found to give erroneous results for charged vacancy defects [12] and/or when distortions are large. When calculating the elastic dipole from the Kanzaki forces, one thus needs to check that these forces correspond to the harmonic regime or the approach has to be extended to take care of anharmonicity [13,14]. On the other hand, Gillan [17,18] popularized the measurement of the elastic dipole components from the strain derivatives of the point-defect formation energy. Subsequent uses of this method or similar ones are numerous, again for defects in both ionics crystals [19] and metals [9,20–23]. Finally, the elastic dipole value can be obtained by extracting from atomistic simulations the displacement field induced by the point defect and by fitting it by the corresponding continuum linear elasticity solution [24].

Most often in the context of *ab initio* simulations, measurements of elastic dipoles or relaxation volumes employ only one of the above methods [9,15,23,25–27]. A recent paper by Nazarov *et al.* [28] shows nevertheless a comparison between the Kanzaki and strain derivatives methods for the hydrogen impurity in hcp zirconium. The authors found significant differences between the methods, although the H solute is a rather simple defect that is known to induce small lattice distortions [29]. Clarifications on the applicability of the different measurement methods in *ab initio* calculations are thus required, even more importantly for the study of defects creating large distortions, like self-interstitial atoms. The convergence of the elastic dipole components with the supercell size is also a point that is not well established in the literature.

*Corresponding author: varvenne@cinam.univ-mrs.fr

In this paper, we first review the different possible approaches to extract elastic dipole tensors from atomistic simulations: strain derivatives of the energy, fitting of the displacement field, and computation from Kanzaki forces. We then provide a systematic comparison of the results obtained with these different approaches. Atomistic simulations relying on empirical potentials are used for this thorough comparison, as they allow for very large simulation sizes and high precision in energy, force, and relaxed atomic positions, which is required to assess the conditions under which each approach must be applied to get consistent results. This is done by considering the vacancy and various configurations of the self-interstitial atom in hcp zirconium. We finally discuss the feasibility of the different methods within *ab initio* calculations, considering the same point defects, and the H impurity in hcp Zr as well. In particular, we show that the strain derivative method, or conversely the residual stress method, is the only one that would give a meaningful result for point defects involving large distortions.

II. METHODS TO EXTRACT ELASTIC DIPOLES

In this section, we recall the necessary background of anisotropic continuum linear elastic modeling of point defects, so as to introduce the concept of elastic dipole. All along the theoretical progress, we detail the different possibilities for their determination into atomistic simulations.

Within continuum elastic theory [1–3], a point defect located at the origin can be represented as a finite distribution of point forces $\{\mathbf{F}^q\}$, acting at positions $\{\mathbf{a}^q\}$. This distribution is at mechanical equilibrium, meaning that there is no force resultant and no net torque:

$$\sum_q \mathbf{F}^q = \mathbf{0}; \quad \sum_q \mathbf{F}^q \times \mathbf{a}^q = \mathbf{0}. \tag{1}$$

The elastic displacement at continuous position $\mathbf{R}$ from the defect is then given by

$$u_i^{\mathrm{el}}(\mathbf{R}) = \sum_q G_{ij}(\mathbf{R} - \mathbf{a}^q) F_j^q, \tag{2}$$

where i, j are Cartesian indexes, and summation over repeated indexes is implicit. $G_{ij}(\mathbf{R})$ is the continuum anisotropic elastic Green's function of the matrix. For large distance R, i.e., $R = \|\mathbf{R}\| \gg \|\mathbf{a}^q\|$, a Taylor expansion of the Green's function can be performed with respect to the $\{\mathbf{a}^q\}$ as

$$\begin{aligned} u_i^{\mathrm{el}}(\mathbf{R}) &= \sum_q \left[G_{ij}(\mathbf{R}) - G_{ij,k}(\mathbf{R}) a_k^q + o(\|\mathbf{a}^q\|) \right] F_j^q \\ &= - G_{ij,k}(\mathbf{R}) P_{jk} + o(\|\mathbf{a}^q\|), \end{aligned} \tag{3}$$

$$\text{with} \quad P_{jk} = \sum_q F_j^q a_k^q. \tag{4}$$

The zeroth-order term in Eq. (3) vanishes because there is no force resultant [Eq. (1)]. The notation "k" stands for the operator $\partial/\partial x_k$ and $G_{ij,k}(\mathbf{R})$ is thus the first derivative of the Green's functions. The tensor P_{jk} is the elastic dipole of the defect, defined as the first moment of the defect force distribution [Eq. (4)]. This tensor is symmetric since the defect has no net torque [Eq. (1)]. Higher-order terms in Eq. (3) would correspond to higher-order moments of the defect force distribution (multipoles), and are neglected here.

Equation (3) provides a first way to determine the elastic dipole tensor in atomistic simulations. After the structural relaxation in a point-defect calculation, the difference between final and initial atomic positions gives atomistic values for the displacement field $\{\mathbf{u}^{\mathrm{at}}(\mathbf{R})\}$ at any atomic position $\mathbf{R}$. The first derivative of the anisotropic elastic Green's function $G_{ij,k}(\mathbf{R})$ can be computed from the elastic constants C_{ijkl} of the bulk matrix, e.g., following the numerical scheme provided by Barnett [30]. A fitting of the atomistic displacement fields using the elastic solution of Eq. (3) will thus allow for an identification of the defect elastic dipole. Such an approach has been followed within empirical potential simulations by Chen *et al.* [24], but with the additional constraint of isotropic elasticity for the computation of the first derivative of the Green's function.

A second approach emerges when considering the interaction energy between the point defect located at the origin, as represented by the finite distribution of point forces, and an external field of arbitrary source. This interaction energy is given by [31]

$$E^{\mathrm{int}} = -P_{ij}\, \varepsilon_{ij}^{\mathrm{ext}}(\mathbf{0}) + o(\|\mathbf{a}^q\|), \tag{5}$$

after a Taylor expansion of the external displacement field, and noting again that the force resultant is null. $\varepsilon_{ij}^{\mathrm{ext}}(\mathbf{0})$ is the external deformation field evaluated at the defect position. This well-established expression allows computing the interaction of a point defect with the strain produced by another defect or with an external applied strain. It also provides a route to identify the elastic dipole tensor in atomistic simulations [9,22]. Let us consider a simulation box of volume V, the equilibrium volume of the defect-free bulk material, containing one point defect and submitted to a homogeneous strain ε_{ij}. According to linear elasticity, the energy of the simulation box is

$$E(\varepsilon_{ij}) = E_0 + E^{\mathrm{D}} + \frac{V}{2} C_{ijkl} \varepsilon_{ij} \varepsilon_{kl} - P_{ij} \varepsilon_{ij}, \tag{6}$$

with E_0 the bulk reference energy and E^{D} the unstrained defect excess energy. We are considering a simulation box with periodic boundary conditions to keep the volume V finite and to prohibit the presence of any surface. E^{D} contains therefore a contribution corresponding to the interaction of the point defect with its periodic images. Within linear elasticity theory, this contribution does not depend on the applied strain ε_{ij}. The average residual stress on the simulation box is thus given by

$$\langle \sigma_{ij} \rangle = \frac{1}{V} \frac{\partial E}{\partial \varepsilon_{ij}} = C_{ijkl} \varepsilon_{kl} - \frac{P_{ij}}{V}. \tag{7}$$

For simulations carried out with fixed periodicity vectors, i.e., with $\varepsilon_{ij} = 0$, the elastic dipole is proportional to the homogeneous residual stress

$$P_{ij} = -V \langle \sigma_{ij} \rangle. \tag{8}$$

This residual stress corresponds to the stress increase, after atomic relaxation, due to the introduction of the point defect in the simulation box. Consequently, if the perfect bulk simulation box experiences a nonzero homogeneous stress, this contribution must be subtracted from the residual stress of the defective supercell to identify the elastic dipole tensor.

This is particularly important for *ab initio* simulations, where finite convergence criteria may lead to non-null stresses for a perfect bulk material at its equilibrium lattice parameters. Note that Eq. (8) is to be related to the dipole tensor measurement first proposed by Gillan [17,18], where the elastic dipole is equal to the strain derivative of the formation energy, evaluated at zero strain. This relation can also be derived by averaging the stress field, as predicted by linear elasticity theory, produced by the point defect, taking explicitly into account the periodic boundary conditions [32].

Finally, a third numerical route is found if one focuses on forces and atomic positions around the point defect. This corresponds to the Kanzaki force approach [10,13,33], which is a discrete elasticity approach. Kanzaki forces are defined as the additional forces applied to the atoms in the neighborhood of the defect, so as to produce the same static displacement field as the defect. In the continuous limit and if the displacements are small, making the harmonic approximation valid, we have an equivalence between the finite distribution of point forces $\{\mathbf{F}^q\}$ and Kanzaki forces. Kanzaki forces are obtained by first relaxing the simulation cell containing the defect and by then removing the defect and restoring the perfect crystal in its vicinity. The Kanzaki forces are the opposite of the atomic forces obtained in this second step, when the system is kept frozen, i.e., without any relaxation. Equation (4) can be used to compute the elastic dipole tensor, with $\{\mathbf{a}^q\}$ the positions of the atoms experiencing a force. Technical details for its application will be given in the next section, when appropriate.

III. VALIDATION OF THE DIFFERENT APPROACHES

We apply in this section the previously described approaches to obtain the elastic dipole tensors of various point defects, modeled through atomic simulations relying on empirical potentials. These energy models have a low computational cost and a high precision in force and atomic position determination, thus allowing for a detailed study without any penalizing limitation on the size of the system. We first present the investigated point defects, and then show and discuss the results obtained with the different definitions of the elastic dipole.

A. Studied defects and simulation details

We study here the vacancy and several configurations of the self-interstitial atom (SIA) in hcp zirconium. Both types of point defects are created under irradiation. Their long-range elastic interaction with the different sinks, in particular the dislocations, controls their clustering and the kinetic evolution of the irradiation microstructure. It has thus macroscopic consequences like irradiation hardening [34], irradiation creep [35–38], or irradiation growth [39–41]. In this context, an accurate measure of the elastic dipoles for both vacancy and SIA defects is of interest. Various *ab initio* studies [9,41–43] showed that several SIA configurations with close energies coexist and must be considered. The unrelaxed structures of the studied defects are represented in Fig. 1: the vacancy (V), and the three most stable SIA configurations, i.e., the basal octahedral (BO), the octahedral (O), and the basal split (BS) for which we consider the variant aligned along the $[2\bar{1}\bar{1}0]$ direction. The symmetry, which is conserved here during structural relaxation, is hexagonal for V and BO, trigonal for O, and orthorhombic for BS. As a consequence, only the diagonal components of the dipole are non-null, with three independent components for BS, and only two for V, BO, and O for which $P_{11} = P_{22}$ in a coordinate system with $\mathbf{e}_1$ and $\mathbf{e}_2$ in the basal plane, respectively, parallel to the $[2\bar{1}\bar{1}0]$ and $[01\bar{1}0]$ directions, and $\mathbf{e}_3$ along the [0001] direction. Those point defects, with various relaxation magnitudes and point symmetries, cover a wide range of situations.

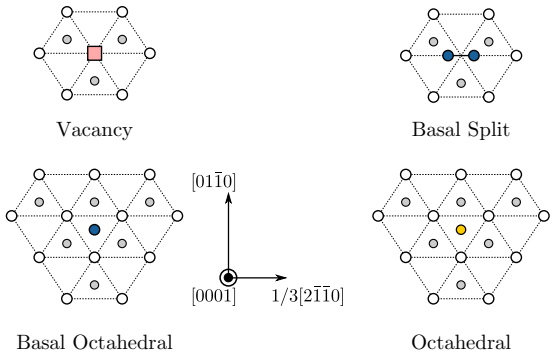

FIG. 1. Projection in the basal plane of the different point defects investigated in hcp Zr: the vacancy and three SIA configurations. The white spheres represent the bulk Zr atoms at $z = 0$, the gray spheres the bulk Zr atoms at $z = c/2$. The square represents the vacancy (V), the blue spheres are SIAs at $z = 0$ (BO and BS configurations), and the yellow sphere the SIA at $z = c/4$ (O configuration).

We select two embedded atom method (EAM) potentials to model Zr, both developed by Mendelev and Ackland [44] and denoted as #2 and #3 in Ref. [44]. A second moment approximation (SMA) potential developed by Willaime and Massobrio [45] is also used and is referred to as WM1 in the following. All potentials give reasonable properties for bulk hcp Zr.[1] The EAM #2 potential was originally designed to describe the hcp-bcc transition, but also gives reasonable defect properties. It accounts for the vacancy-vacancy binding but underestimates stacking fault and surface energies [46]. The EAM #3 potential is supposed to be well suited to study defects in the hcp phase, as some stacking fault energies were adjusted on *ab initio* calculations. It has been used for the computation of the properties of vacancy, SIAs, and clusters [47]. However, it does not account for the binding between vacancies [46]. The WM1 SMA potential was also developed to describe the hcp-bcc transition. It has a lower cutoff radius than the two EAM potentials, and is chosen for discussion purposes.

Atomistic simulations with these many-body potentials are performed on supercells containing up to 12 800 atomic sites (i.e., $20 \times 20 \times 16$ hcp primitive unit cells), which ensures well-converged defect energetics and is sufficiently large to define well-converged elastic dipoles with any of the previously introduced methods. Note that periodicity vectors are kept fixed during the structural relaxations, and also in the eventual additional calculations required for elastic dipole tensor computation.

[1]Note that WM1 elastic constants are unrelaxed in Ref. [45].

TABLE I. Elastic dipoles of the vacancy (V), of the BO, O, and BS configurations of the SIA, and of the H solute in tetrahedral position in hcp Zr. In the chosen coordinate system, with $\mathbf{e}_1 \parallel [2\bar{1}\bar{1}0]$, $\mathbf{e}_2 \parallel [01\bar{1}0]$, and $\mathbf{e}_3 \parallel [0001]$, all tensors are diagonal. The dipole components have been obtained either by a fitting of the displacement field, by the computation of the Kanzaki forces, or from the residual stress. Results are given in eV, for different empirical potentials, EAM #2 and #3 from Ref. [44], and SMA WM1 from Ref. [45], and for *ab initio* calculations. P_{ij} values are obtained using $N = 12\,800$ atoms supercells for empirical potentials (except the displacement method, on 1600 atoms supercells), and from $1/N \to 0$ extrapolation for *ab initio* calculations.

		V		BO		O		BS			H	
Potential	Method	P_{11}	P_{33}	P_{11}	P_{33}	P_{11}	P_{33}	P_{11}	P_{22}	P_{33}	P_{11}	P_{33}
EAM #2	Kanzaki	−0.67	−0.79	13.8	5.85	11.5	8.30	13.5	14.8	6.6		
	Residual stress	−0.65	−0.79	14.0	6.00	11.6	8.36	13.6	14.8	6.6		
EAM #3	Displacement	−5.45	−5.55	11.8	6.15	15.3	16.2					
	Kanzaki	−5.41	−5.51	11.8	6.35	15.6	16.5	13.6	11.6	8.2		
	Residual stress	−5.43	−5.51	11.7	6.32	15.5	16.4	13.5	11.6	8.2		
SMA WM1	Kanzaki	−4.28	−4.34	30.2	16.8	24.4	29.3	31.1	29.9	15.5		
	Residual stress	−4.27	−4.33	30.5	16.9	24.5	29.5	31.3	30.2	15.6		
Ab initio	Residual stress	−5.14	−7.62	17.0	10.6	14.9	17.0	14.2	22.1	9.3	1.74	2.92

B. Validation of the residual stress method

We first identify the elastic dipole from the residual stress measured in the simulation box after introduction of the point defect and relaxation of the atomic positions [Eq. (8)] using the virial stress [48,49] given by the atomic simulations. The values obtained for the different point defects and using the different empirical potentials are given in Table I. These values are well converged: no difference larger than 5×10^{-3} eV is observed when going from a simulation cell containing 1600 atoms to one with 12 800 atoms. To validate the values thus obtained, we compare the interaction energy of the point defect with an applied homogeneous strain, as predicted by the elasticity theory [see Eq. (5)] using this elastic dipole, with the result given by direct atomistic calculations. In these simulations, the interaction energy is defined as

$$E^{\text{int}}(\varepsilon_{ij}) = E^{\text{PD}}_{\varepsilon_{ij}} - E^{\text{bulk}}_{\varepsilon_{ij}} + E^{\text{bulk}}_{0} - E^{\text{PD}}_{0}, \tag{9}$$

with $E^{\text{PD}}_{\varepsilon_{ij}}$ and $E^{\text{bulk}}_{\varepsilon_{ij}}$ the energies of the strained defective and bulk supercells, and with E^{PD}_{0} and E^{bulk}_{0} the energies of the unstrained defective and bulk supercells, respectively. Results of the comparison are shown in Fig. 2 for two different deformations: a dilatation ($\varepsilon_{ij} = \varepsilon\,\delta_{ij}$) and a pure shear ($\varepsilon_{11} = -\varepsilon_{33} = \varepsilon$ with all other components set to zero). A very good agreement is found between elasticity theory and atomistic simulations for all investigated defects. The interaction energy predicted by atomistic simulations starts to deviate from the linear behavior predicted by elasticity theory only for the dilatation when the applied strain gets too high, close to ±2%. This therefore validates the measurement of the elastic dipole tensor from the defect-induced residual stress in the simulation box. Similar validations can be found in Refs. [5,27]. We will thus use the value obtained from the residual stress as a reference for the elastic dipole when comparing with other methods.

C. Displacement field approach

We now consider the method identifying the elastic dipole through the displacement field. The elastic dipole components are obtained from the displacement field $\{\mathbf{u}^{\text{at}}(\mathbf{R})\}$ extracted from atomistic simulations through a least-square fitting using the cost function

$$f(P_{ij}) = \sum_{\substack{\mathbf{R} \\ \|\mathbf{R}\| > r_{\text{excl}}}} \|R^2[\mathbf{u}^{\text{el}}(\mathbf{R}) - \mathbf{u}^{\text{at}}(\mathbf{R})]\|^2, \tag{10}$$

with r_{excl} the radius of a small spherical zone around the point defect, so as to exclude from the fitting the atomic positions where elasticity does not hold. The R^2 factor is meant to account for the scaling of the elastic displacements with the distance R to the defect, i.e., to give a similar weight to all atomic positions in the fitting. Without this R^2 penalty, the obtained P_{ij} values are entirely fixed by the displacements at the neighbor shell bordering the exclusion zone. Due to the periodic boundary conditions used in atomic simulations, we need to include the contribution of the defect periodic images into the elastic displacements $\{\mathbf{u}^{\text{el}}(\mathbf{R})\}$, that are now given by

$$u_i^{\text{el}}(\mathbf{R}) = -\sum_{n,m,p} G_{ij,k}(\mathbf{R} - \mathbf{R}_{nmp}) P_{jk}, \tag{11}$$

with $\mathbf{R}_{nmp} = n\mathbf{A_1} + m\mathbf{A_2} + p\mathbf{A_3}$ the positions of the supercell periodic images, with n, m and $p \in \mathbb{Z}$, and $\mathbf{A_1}$, $\mathbf{A_2}$, and $\mathbf{A_3}$ the periodicity vectors of the supercell. $G_{ij,k}(\mathbf{R})$ is computed using Barnett's numerical scheme [30]. The summation involved in Eq. (11) is conditionally convergent and is regularized using the procedure of Cai *et al.* [50]. With this, the cost function f can be accurately evaluated for any trial values of the elastic dipole P_{ij} and the fitting is realized. We have assumed in Eqs. (10) and (11) that the point defect is located at the origin, but the exact position of the point defect can also be included in the cost function to be obtained then from the least-square fitting.

The resulting elastic dipole tensor components for the vacancy and the BO and O configurations of the SIA are shown in Fig. 3 as a function of the exclusion zone radius for the EAM #3 potential. Two different simulation box sizes are tested: a large one with 1600 atomic sites and a smaller one with 200 sites. With the largest simulation box, the choice of r_{excl} has

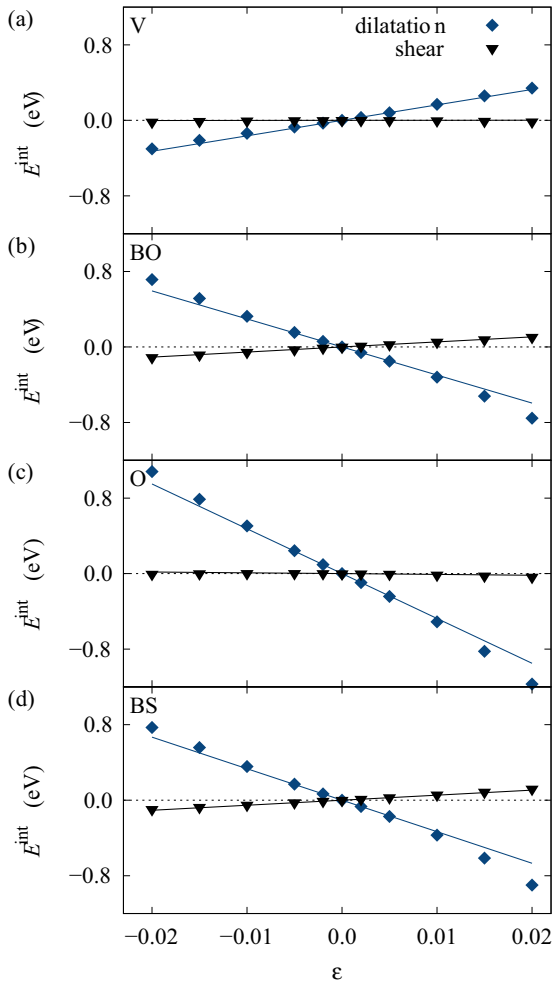

FIG. 2. Interaction energy between (a) V, (b) BO, (c) O, and (d) BS point defects and homogeneous applied strains corresponding either to dilatation or pure shear. Filled symbols are the results of atomistic simulations and straight lines the predictions of elasticity theory [Eq. (5)] using the elastic dipole deduced from the residual stress [Eq. (8)]. Data have been obtained with the EAM #3 potential.

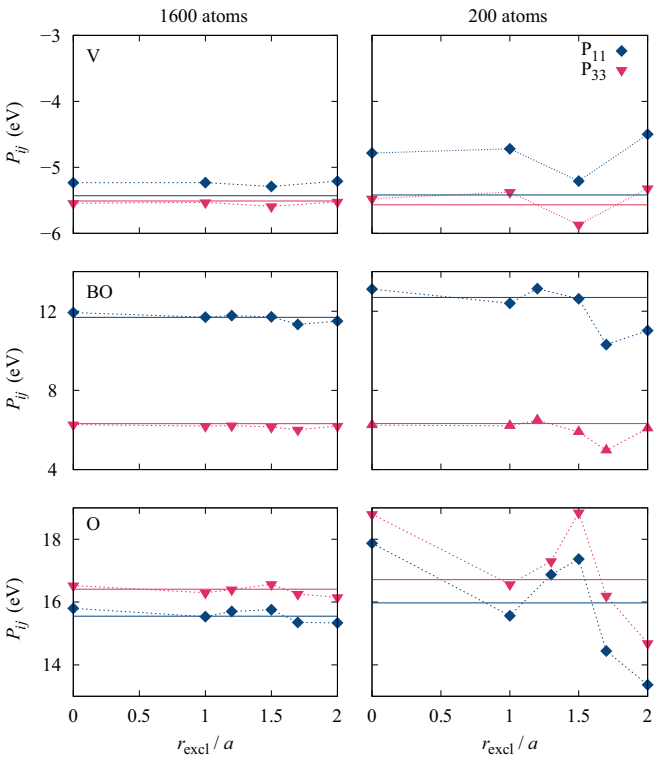

FIG. 3. Elastic dipole components P_{11} and P_{33} for the vacancy, and the BO and O configurations of the SIA, obtained through a fitting on the atomistic displacement, versus the radius of the exclusion zone r_{excl} normalized by the lattice parameter a. The horizontal lines indicate the values deduced from the residual stress. The simulation boxes used for both displacement field and residual stress approaches contain 1600 (left side) and 200 atoms (right side).

almost no influence on the final value of the elastic dipole components, for all defect types. Numerical values of the P_{ij} for $r_{excl} = 2a$ are given in Table I for each defect. In fact, the number of atomic positions included in the fit, and for which elasticity is valid, is sufficiently high to avoid issues arising from the defect core zone. On the other hand, for the smaller simulation box, the obtained elastic dipole components are highly sensitive to r_{excl}, and their convergence with r_{excl} cannot be reached. This is especially true for the SIAs because of the larger induced distortions. For this small size of the simulation box, higher r_{excl} values cannot be used, as the number of remaining atoms to be included into the fit becomes too small to obtain a meaningful value of the P_{ij} tensor. This convergence issue preventing the determination of an appropriate r_{excl} will become even more important for complex and larger defects, such as point-defect clusters. This disqualifies the use of this displacement method to obtain elastic dipoles from *ab initio* calculations, as the typical simulation box sizes are limited to a few hundred atoms.

D. Kanzaki force method

We now focus on the Kanzaki force method, that uses Eq. (4) to obtain P_{ij}. To compute the defect-induced forces, we follow the procedure given in Refs. [14,16], which is illustrated for a vacancy in Fig. 4. Starting from the relaxed structure of the point defect [Fig. 4(b)], we restore the perfect lattice in the defect core, e.g., we add back the suppressed atom for the vacancy case of Fig. 4(c) and then perform a static force computation on all atoms of the obtained simulation cell. These forces are used to compute the elastic dipole $P_{ij} = \sum_q F_i^q a_j^q$, where $\mathbf{F}^q$ is the force acting on atom located at $\mathbf{a}^q$, assuming the point defect at the origin. The summation is restricted to atoms located inside a sphere of radius r_∞ (i.e., $\|\mathbf{a}^q\| < r_\infty$). As the Kanzaki technique is valid only in the harmonic approximation, one also needs to check that the atomic forces entering the elastic dipole definition are in the harmonic regime [14]. This is done by restoring larger and larger defect neighboring shells to their perfect bulk positions, and computing the forces on the obtained restored structures [Figs. 4(c) and 4(d)] before defining the elastic dipole. The case where n defect neighbor shells are restored is referred to as the nth-order approximation. As the restored zone becomes larger, the atoms remaining at their relaxed positions are more likely to sit in a harmonic region. The convergence of the resulting elastic dipole components with respect to the restoration zone radius thus enables to evaluate the harmonicity aspect.

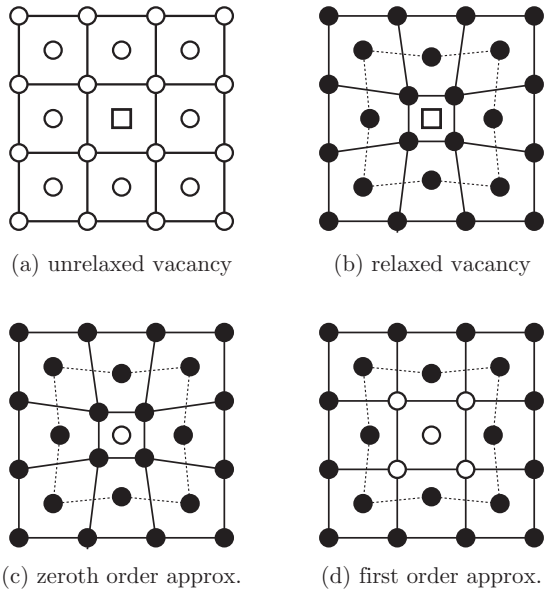

FIG. 4. Schematic illustration of the procedure used for the computation of the Kanzaki forces in the case of a vacancy defect. The white spheres correspond to atoms at their perfect bulk positions, i.e., before relaxation, the white square to the vacancy defect, and the black spheres to the atoms at their relaxed position around the defect.

We first consider the zeroth-order approximation, where only the atom corresponding to the point defect is restored. Figure 5 provides the elastic dipole values obtained with the EAM #3 potential for the vacancy and the three configurations of the SIA. Results are shown as a function of the cutoff radius r_∞ used for the summation. This allows to determine the range of the defect-induced forces. For all defects, constant P_{ij} values are reached for $r_\infty \simeq 2{-}2.5a$, which corresponds to $\sim$10$-$13 defect neighboring shells included in the P_{ij} calculations. The last forces entering the summation and needed to reach a $\sim$0.1 eV precision for the P_{ij} elastic dipole are only a few meV/Å, a small value that requires a high precision in the force calculation. The rather long-range behavior of the defect-induced forces is also observed with the two other empirical potentials. In particular, although the WM1 potential has a lower cutoff than EAM #2 and #3 potential, it leads to longer-range defect-induced forces. This long-range nature of these forces is not specific to hcp Zr as it has also been observed in the case of SIA defect in bcc iron [16]. Note, finally, that the P_{ij} values obtained with this zeroth-order approximation do not always correspond to the values obtained by the residual stress method (Fig. 5): this is especially true for the O and BS configurations of the SIA.

We study now the effect of anharmonicity by increasing the size of the defect restoration zone, going thus beyond this zeroth-order approximation. We use, in the force summation, a cutoff radius r_∞ high enough to ensure convergence with respect to this parameter. The value needed for this cutoff radius increases with the order n of the approximation used for the restoration zone. As a consequence, the precision on the atomic forces also needs to be increased. As can be seen in Fig. 6(a), the vacancy elastic dipole components are already well converged for the zeroth-order approximation, meaning

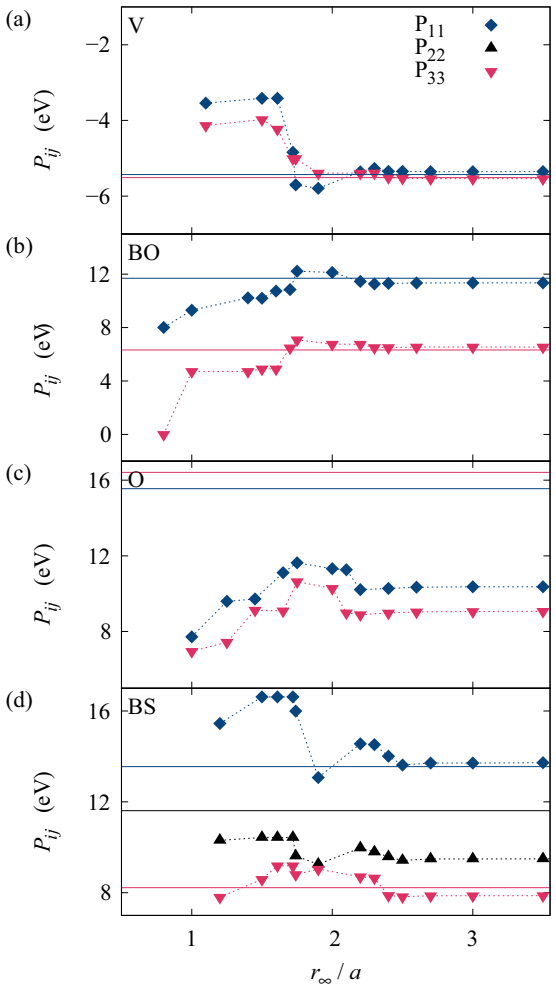

FIG. 5. Convergence of the elastic dipole components with the cutting radius r_∞ of the force summation [Eq. (4)] for the Kanzaki method. The elastic dipoles are calculated in the zeroth-order approximation for the vacancy and the BO, O, and BC configurations of the SIA, using EAM #3 potential. The horizontal lines indicate the values deduced from the residual stress method.

that the harmonic approximation is valid very close to the defect position in this case. On the other hand, this is not true for the different configurations of the SIA [Figs. 6(b)–6(d)]. Converged values are obtained only for restoration zones extending a few lattice distances from the point defect ($\geqslant 2a$). The zeroth-order approximation can be sometimes completely wrong. This is the case for instance for the O configuration for which the magnitude of the elastic dipole components are $\sim$50% off as compared to the converged values, and the relative magnitude of P_{11} and P_{33} is reversed. The BS configuration presents an interesting feature, as the size of the necessary restoration zone is $\sim 4a$ for P_{11}, $\sim 2a$ for P_{22}, and $\sim 3a$ for P_{33}. This thus defines the anisotropic dimensions of the point-defect core zone, which, within an Eshelby's inclusion model [51], corresponds to the dimensions of the principal axes of the ellipsoidal inclusion. Similar behaviors are found with the two other empirical potentials, with a small anharmonicity for the vacancy with WM1 potential. When defining the elastic dipoles from Kanzaki forces, one therefore needs to adapt

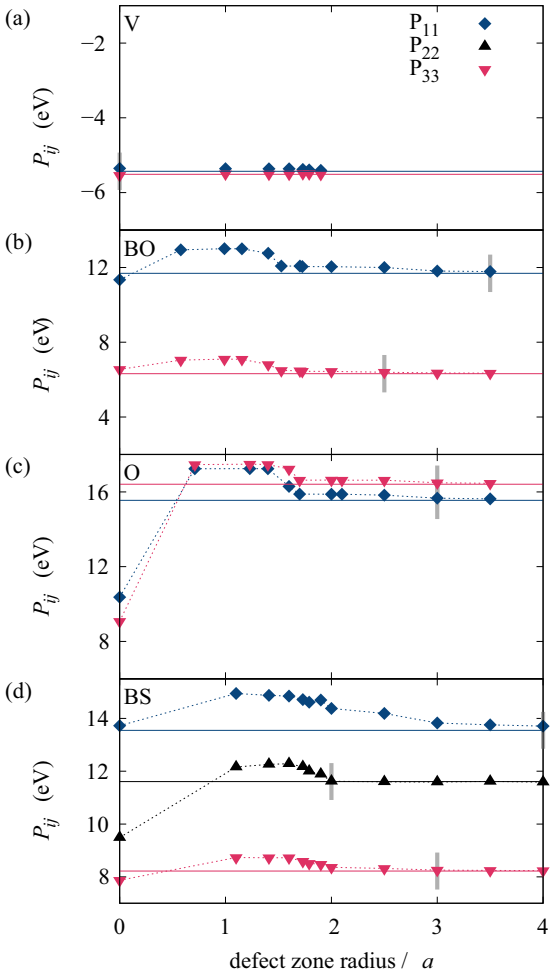

FIG. 6. Convergence of the elastic dipole components with the radius of the defect restoration zone for the Kanzaki method. The elastic dipoles are calculated for the vacancy and the BO, O, and BS configurations of the SIA, using EAM #3 potential. The horizontal lines indicate the values deduced from the residual stress method. The vertical gray tics indicate the converged values of the defect restoration radii, corresponding to the point-defect core zone dimensions.

the restoration zone to include the anharmonic region around the point defect. As this anharmonic region depends on the defect and on the material, one cannot choose *a priori* an approximation order for the restoration zone, but one needs to check the convergence of the elastic dipole with the size of this restoration zone.

E. Discussion

Table I provides the elastic dipole components for all studied point defects, obtained with the three different empirical potentials, and measured by the different techniques. The Kanzaki method values correspond to those converged with respect to the defect restoration zone size and to the cutoff radius of the force summation. Displacement field values are those obtained with the largest simulation box, which is sufficient to provide P_{ij} values converged with respect to the supercell size, as tested by the residual stress method. The three approaches give the same results for the elastic dipole tensors of all point defects. This confirms the coherence of the elastic dipole definition and its link to the point-defect stress field and energetics. As an aside, we note that comparison between the different interatomic potentials for a given defect shows important variations of the obtained elastic dipoles, with differences of several eV and eventually different relative magnitudes between the different dipole components. Although some properties of the point defects were considered in the fitting of these empirical potentials, they lead to completely different pictures of the long-range elastic field induced by these point defects. It is therefore difficult to rely on any of them, and this motivates the need for *ab initio* computations to obtain quantitative estimates of the P_{ij} elastic dipoles.

We now discuss practical aspects of the different methods which can be used to determine P_{ij}. For the fitting of the displacement field, one drawback is the necessity to check the sensitivity of the result to the parameter defining the exclusion zone around the defect and, also, to a less extent, to the initial conditions. But most importantly, the method is not operative for small supercells that are typically tractable in *ab initio* simulations. On the other hand, the method offers the advantage that the exact position of the point defect does not need to be known *a priori* since it is determined through the fitting. This is not true anymore when the elastic dipole is defined from the Kanzaki forces. The defect position must then be known so as to properly restore the defect zone and compute the atomic positions $\{\mathbf{a}^q\}$ entering in the definition of the dipole. Knowing the defect position is usually easy for high-symmetry defects, but can be more tricky for point defects with lower symmetry, e.g., small amorphous zones. Another drawback of the method is that additional calculations are required to obtain the Kanzaki forces and to check that the forces entering the dipole definition are in the harmonic regime. The residual stress method appears therefore as the easiest and fastest one to obtain accurate values of the elastic dipole. It only uses the virial stress on the simulation box, which is a standard output from any atomistic code, either relying on empirical potentials or *ab initio*, and the defect position is not needed. With this method, no post treatment nor additional calculations are required to obtain an accurate value of the elastic dipole.

We finally comment on additional point-defect characteristics that are outcomes of some of the P_{ij} extraction techniques. We first notice that the point-defect higher-order multipoles, corresponding to the higher-order terms in the expansion of Eq. (3), are accessible by both Kanzaki's and displacement field methods[2] but not from the defect residual stress. Their contribution in the interaction energy between the point defect and an external strain field involves successive gradients of the strain. It is thus much shorter range than the dipole contribution [3,31], and direct atomistic calculations are usually preferred to the use of these higher-order elasticity models. Second, and as pointed out in the previous section, Kanzaki's technique

[2]Directly from the forces and position values after getting rid of anharmonicity for the Kanzaki technique, and by including the multipole terms in the fitting function for the displacement method.

has the special feature of providing a physically founded determination of the size and the shape of the defect core zone, based on the analysis of anharmonicity. This could be valuable in the context of Eshelby's inclusion models used for mesoscopic simulations of amorphous plasticity [52], where a key step is the atomic-scale identification of the size of the inclusion equivalent to each plastic event, and that would become unambiguous by adapting Kanzaki's procedure.

IV. APPLICATION TO *AB INITIO* COMPUTATIONS

We now consider extraction of elastic dipole tensors from *ab initio* calculations, that are usually limited to a few hundred atoms. As previously established using empirical potentials, the displacement field method is not reliable for these small supercells and is thus left out. We study the same point defects in hcp Zr as with empirical potentials, plus the hydrogen solute, an interstitial impurity occupying the tetrahedral sites [53,54], and that induces smaller distortions than both the vacancy and the SIA.

A. Computational details

Our *ab initio* calculations are based on the density functional theory (DFT), as implemented in the PWSCF code of the QUANTUM ESPRESSO package [55]. Calculations are performed in the generalized gradient approximation with the exchange-correlation functional of Perdew, Burke, and Ernzerhof [56]. Valence electrons are described with plane waves, using a cutoff of 28 Ry. The pseudopotential approach is used to describe the electron-ion interaction. For Zr and H, ultrasoft pseudopotentials of Vanderbilt type have been chosen, including $4s$ and $4p$ electrons as semicore in the case of Zr. The electronic density of states is broadened with the Methfessel-Paxton function, with a broadening of 0.3 eV. The integration is performed on a regular grid of $14 \times 14 \times 8$ **k** points for the primitive cell and an equivalent density of **k** points for larger supercells. This choice of cutoffs, **k** mesh, GGA functional for the exchange correlation, and pseudopotential for Zr and H have already been validated on the hcp bulk, on vacancy cluster properties and on hydrogen-vacancy defect interactions in previous studies [9,46,57,58].

To compare the Kanzaki and residual stress methods for the various defects, we use supercells of $6 \times 6 \times 5$ repeated hcp unit cells (i.e., 360 atoms), with full periodic boundary conditions. Atomic relaxations are performed at constant volume, using a conjugate gradient algorithm. The force tolerance is 1.5 meV Å^{-1} for the H solute, and 5 meV Å^{-1} for the vacancy and the SIA. Note that in the Kanzaki force technique, all the measured defect-induced forces that are lower than the tolerance for ionic relaxation were set to zero for the elastic dipole tensor calculation. When defining the dipole tensor from the residual stress, we subtract from the stress of the defective supercell the stress of the perfect crystal for the same supercell. Although this last contribution should be zero in theory for a relaxed crystal, a remaining stress exists in the perfect crystal because of the wave-function-basis incompleteness. Withdrawing this remaining stress from the defective supercell allows compensating numerical errors associated with *ab initio* calculations and accounting only for the stress variation associated with the introduction of the point defect.

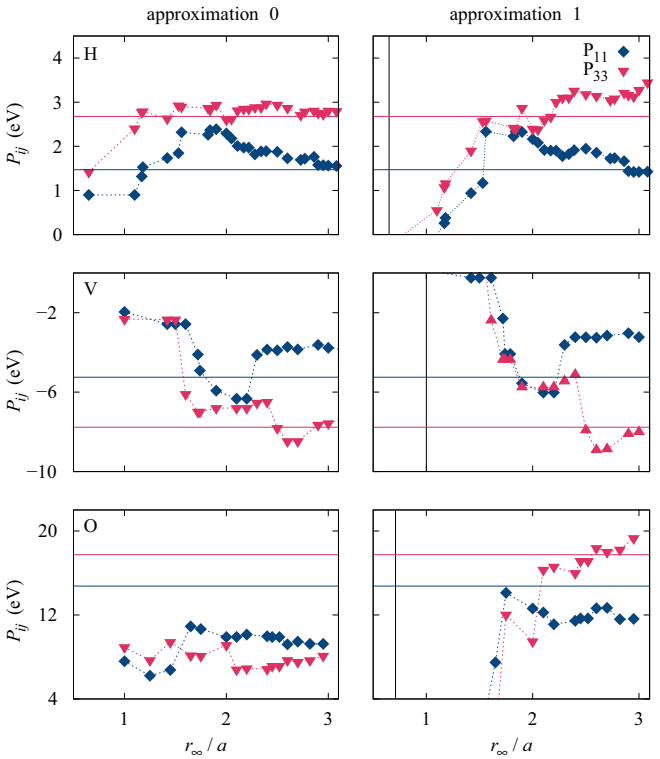

FIG. 7. Convergence of the elastic dipole components obtained from the Kanzaki forces with the cutting radius r_∞ of the force summation [Eq. (4)], for the H solute atom, the vacancy, and the O configuration of the SIA, computed using *ab initio* calculations. When computing the Kanzaki forces, only the point defect is restored in the left figures (approximation 0), whereas the first-neighbor shell is also restored in the right figures (approximation 1). The horizontal lines indicate the values deduced from the residual stress and the vertical lines the radius of the restoration zone.

B. Kanzaki vs residual stress method

Figure 7 displays the elastic dipole tensors obtained either from the Kanzaki forces or from the residual stress for defects of increasing relaxation magnitudes: the H impurity, the vacancy, and the O configuration of the SIA.

When the zeroth-order approximation is used, i.e., when the Kanzaki forces are calculated after a simple removal of the point defect, the elastic dipole obtained from the summation on the atomic forces converges to the value deduced from the residual stress only for the H impurity. The agreement between both methods is good only for the P_{33} component for the vacancy defect, and for none of the dipole components for the SIA. Going to the first-order approximation and restoring the first nearest neighbors of the point defect, the summation of the Kanzaki forces leads to an elastic dipole closer to the value deduced from the residual stress for the SIA. But, it does not change the values for the vacancy and indeed worsens the agreement for the H impurity. With this first-order approximation, the convergence of the elastic dipole with the range of the Kanzaki forces, i.e., with the truncation radius r_∞

of the force summation, is hardly achieved. This is especially true for the P_{33} component, whatever the point defect. As previously underlined in empirical potential calculations, the range of the defect-induced forces increases with the radius of the restoration zone, and the last force to sum up in the dipole calculation becomes smaller. This makes it difficult to reach a converged value with *ab initio* calculations because of the small size of the supercell and of the finite precision which can be obtained on atomic forces. Consequently, increasing further the size of the defect restoration zone is not a practicable solution to get rid of anharmonicity and obtain well-converged values, even for very simple point defects like the H impurity and the vacancy. The definition of the elastic dipole from the residual stress appears therefore as the only method leading to reliable values within *ab initio* calculations.

C. Variation with supercell size

One remaining question is how sensitive is the elastic dipole to the size of the supercell. Defining now the elastic dipole only from the residual stress, we study its variations with the supercell size for the H impurity, the vacancy, and the three configurations of the SIA. As shown in Fig. 8, important variations are seen between the smallest supercell which contains only 32 lattice sites and the larger ones. But, the obtained values are quite constant above a given size, above 96 lattice sites for the defect-inducing small relaxations (H and V) and above 200 lattice sites for the SIA. Such a variation of the elastic dipole at the small sizes arises from the interaction of the point defect with its periodic images. Because of the polarizability of the point defect [59–61], its elastic dipole may depend on the strain seen by the point defect, and thus on the strain created by its periodic images. As the strain created by a point defect is varying as $1/r^3$, the polarizability associated with the periodic boundary conditions leads to a value of the elastic dipole which converges with the inverse of the supercell volume [23,62]. This corresponds to the behavior observed in our simulations (see insets in Fig. 8), and taking the limit $1/N \to 0$ with N the number of atoms in the supercell, or similarly $1/V \to 0$, leads to a converged value of the elastic dipole (see Table I for numerical values).

Regarding finally the largest supercell size for the H impurity and the vacancy, a decrease of the P_{ij} values is seen. For these defects with small elastic dipoles, the residual stress needed to compute the elastic dipole becomes very small for the 360 atom supercell, less than 40 MPa for the smallest component of the elastic dipole ($P_{11} \simeq 1.5$ eV for H). Obtaining a higher precision on the stress places high requirement in convergence criterion for the electronic density and in the tolerance on forces for ionic relaxation. This would then result in an important increase of computational time for these defect computations. A compromise needs therefore to be found to limit the polarizability influence observed at small sizes and the stress precision problem inherent to large sizes.

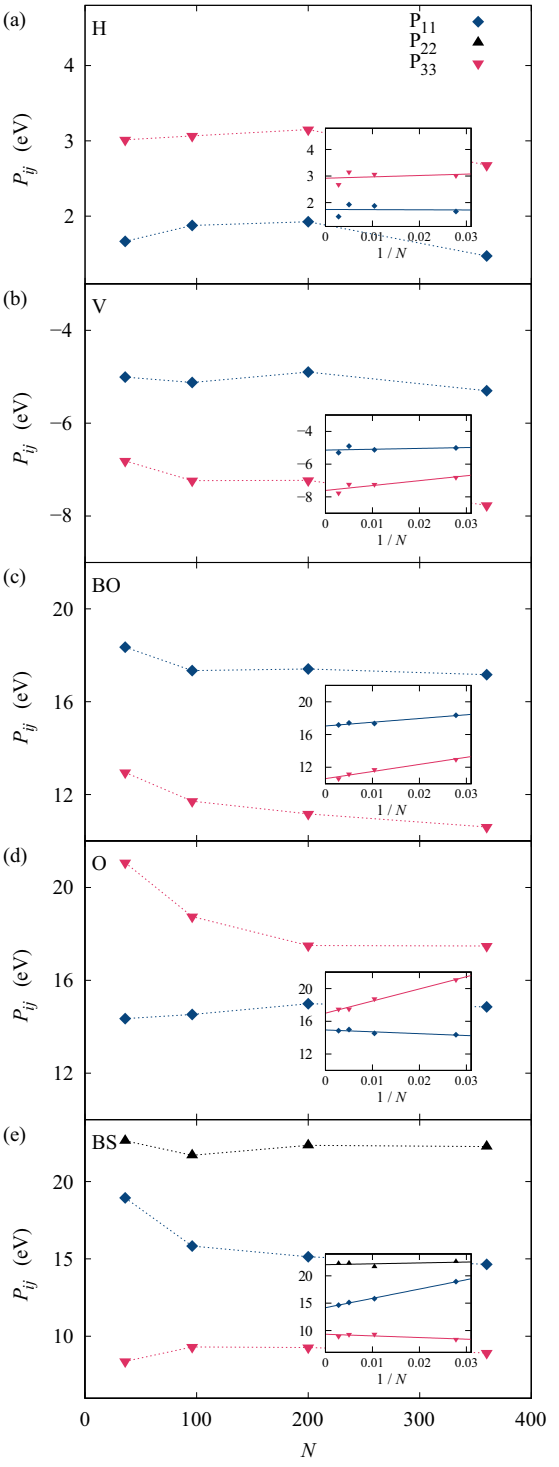

FIG. 8. Convergence of the elastic dipole components deduced from the residual stress computed by DFT with N the number of atoms in the supercell for (a) the H impurity, (b) the vacancy, and (c) the BO, (d) O, and (e) BS configurations of the SIA. The insets show the variation of the elastic dipoles with the inverse of N, with the straight line corresponding to the $1/N$ interpolation.

D. H solute: Comparison with experiments

As already noted by Domain *et al.* [29] and by Nazarov *et al.* [28], the elastic dipole for H impurity deduced from *ab initio* calculations only partly agrees with experiments. Mac Ewen *et al.* [63] observed in Zr an anisotropic expansion varying linearly with the hydrogen atomic fraction x_H and

characterized by the two coefficients

$$\lambda_a = \frac{1}{a}\frac{\partial a}{\partial x_{\mathrm{H}}} \quad \text{and} \quad \lambda_c = \frac{1}{c}\frac{\partial c}{\partial x_{\mathrm{H}}}.$$

They measured $\lambda_a = (3.17 \pm 0.38) \times 10^{-2}$ and $\lambda_c = (5.19 \pm 0.46) \times 10^{-2}$ at 727 K, and close values at 777 K. These two coefficients are simply related to the elastic dipoles as

$$\lambda_a = \frac{1}{\Omega}\frac{C_{33}P_{11} - C_{13}P_{33}}{(C_{11}+C_{12})C_{33} - 2{C_{13}}^2},$$
$$\lambda_c = \frac{1}{\Omega}\frac{-2C_{13}P_{11} + (C_{11}+C_{12})P_{33}}{(C_{11}+C_{12})C_{33} - 2{C_{13}}^2},$$

where $\Omega = \sqrt{3}a^2c/4$ is the atomic volume. Using the experimental elastic constants measured at 723 K [64] and the lattice parameters measured at 700 K [65], our *ab initio* values of the elastic dipole for H determined at 0 K ($P_{11} = 1.74$ and $P_{33} = 2.92$ eV) lead to $\lambda_a = 2.4 \times 10^{-2}$ and $\lambda_c = 11.2 \times 10^{-2}$. Like previous *ab initio* studies [28,29], we obtain a reasonable agreement for the dilatation in the $\langle a \rangle$ direction and overestimate the dilatation in the $\langle c \rangle$ direction. As mentioned by Nazarov *et al.* [28], part of the discrepancy may arise from limitations of the GGA functional to describe interaction between Zr and H atoms. A variation with the temperature of the elastic dipole components, deviating from their 0-K value, is also possible. Finally, one should not forget that these theoretical values have been obtained by assuming that H atoms only occupy the tetrahedral interstitial sites, in agreement with neutron diffraction experiments performed at room temperature [53] and inelastic neutron scattering performed at 873 K [54]. But, recent *ab initio* calculations [46,66] have shown that the difference in energy between the tetrahedral and octahedral (O) interstitial sites is small enough to allow for a non-negligible occupation also of the O sites at finite temperature. A proper description of the variations with temperature of the H concentrations in the different possible insertion sites necessitates to include vibrations. The harmonic approximation is not sufficiently precise for this purpose [46], making difficult their computation. The experimental values of the lattice expansion induced by H solute atoms measured at 727 and 777 K could therefore hardly be compared to 0-K static *ab initio* calculations in the case of H solute.

V. CONCLUSIONS

The different possible methods to extract elastic dipoles of point defects from atomistic simulations have been compared. These elastic dipoles can be obtained from a fitting of the displacement field, a summation of the Kanzaki forces or directly from the residual stress. Using various empirical potentials, we established that, as long as they are carefully applied, i.e., in a context where the harmonic approximation is valid and with large enough supercells, all methods lead to the same elastic dipole values, and this for all the investigated defects. The definition of the elastic dipole from the residual stress appears nevertheless as the most convenient one, as it does not require any additional calculations and does not need to know the defect position. Besides, it leads to quantitative estimates of the elastic dipoles even in small supercells compatible with *ab initio* calculations, in contrast to the methods based on the displacement field or the Kanzaki forces which are not tractable for such small supercells. The definition from the residual stress appears therefore as the best way to extract the elastic dipole from atomistic simulations, in particular from *ab initio* calculations. By doing such calculations for different applied strains, one can also easily study the variation of this elastic dipole with the applied strain and thus extract the diaelastic polarizability of the point defect [59,60,67], another key quantity useful for instance to describe physical phenomena involving the point defect and a coupling between the strain fields originating from two different sources.

ACKNOWLEDGMENTS

Support for this work was provided by national HPC resources from GENCI-CCRT, through the Grants No. 2016-096847 and No. 2017-910165. C.V. thanks W. A. Curtin for useful discussions.

[1] G. Leibfried and N. Breuer, *Point Defects in Metals I*, Springer Tracts in Modern Physics (Springer, Berlin, 1978), Vol. 81.
[2] D. J. Bacon, D. M. Barnett, and R. O. Scattergood, Prog. Mater. Sci. **23**, 51 (1980).
[3] C. Teodosiu, *Elastic Models of Crystal Defects* (Springer, Berlin, 1982).
[4] R. G. A. Veiga, M. Perez, C. S. Becquart, E. Clouet, and C. Domain, Acta Mater. **59**, 6963 (2011).
[5] G. Subramanian, D. Perez, B. P. Uberuaga, C. N. Tomé, and A. F. Voter, Phys. Rev. B **87**, 144107 (2013).
[6] R. Agarwal and D. R. Trinkle, Phys. Rev. B **94**, 054106 (2016).
[7] D. R. Trinkle, Philos. Mag. **96**, 2714 (2016).
[8] A. Vattré, T. Jourdan, H. Ding, M.-C. Marinica, and M. J. Demkowicz, Nat. Commun. **7**, 10424 (2016).
[9] C. Varvenne, F. Bruneval, M.-C. Marinica, and E. Clouet, Phys. Rev. B **88**, 134102 (2013).
[10] V. K. Tewary, Adv. Phys. **22**, 757 (1973).
[11] I. D. Faux and A. B. Lidiard, Z. Naturforsch. **26a**, 62 (1971).
[12] A. B. Lidiard, Philos. Mag. A **43**, 291 (1981).
[13] H. R. Schober and K. W. Ingle, J. Phys. F: Met. Phys. **10**, 575 (1980).
[14] G. Simonelli, R. Pasianot, and E. J. Savino, Phys. Rev. B **50**, 727 (1994).
[15] C. Domain, C. S. Becquart, and J. Foct, Phys. Rev. B **69**, 144112 (2004).
[16] E. Hayward, C. Deo, B. P. Uberuaga, and C. N. Tomé, Philos. Mag. **92**, 2759 (2012).
[17] M. J. Gillan, Philos. Mag. A **43**, 301 (1981).
[18] M. J. Gillan, Philos. Mag. A **48**, 903 (1983).
[19] M. P. Puls, Philos. Mag. A **51**, 893 (1985).
[20] M. W. Finnis and M. Sachdev, J. Phys. F: Met. Phys. **6**, 965 (1976).

[21] P. H. Dederichs, C. Lehmann, and A. Scholz, Z. Phys. B **20**, 155 (1975).
[22] E. Clouet, S. Garruchet, H. Nguyen, M. Perez, and C. S. Becquart, Acta Mater. **56**, 3450 (2008).
[23] E. Clouet, L. Ventelon, and F. Willaime, Phys. Rev. B **84**, 224107 (2011).
[24] Z. Chen, N. Kioussis, N. Ghoniem, and D. Seif, Phys. Rev. B **81**, 094102 (2010).
[25] S. Vannarat, M. H. F. Sluiter, and Y. Kawazoe, Phys. Rev. B **64**, 224203 (2001).
[26] G. P. M. Leyson, L. G. Hector, Jr., and W. A. Curtin, Acta Mater. **60**, 3873 (2012).
[27] T. Garnier, V. R. Manga, P. Bellon, and D. R. Trinkle, Phys. Rev. B **90**, 024306 (2014).
[28] R. Nazarov, J. S. Majevadia, M. Patel, M. R. Wenman, D. S. Balint, J. Neugebauer, and A. P. Sutton, Phys. Rev. B **94**, 241112 (2016).
[29] C. Domain, R. Besson, and A. Legris, Acta Mater. **50**, 3513 (2002).
[30] D. M. Barnett, Phys. Status Solidi B **49**, 741 (1972).
[31] R. Siems, Phys. Status Solidi **30**, 645 (1968).
[32] R. C. Pasianot, Philos. Mag. Lett. **96**, 447 (2016).
[33] H. Kanzaki, J. Phys. Chem. Solids **2**, 24 (1957).
[34] F. Onimus and J. L. Béchade, in *Comprehensive Nuclear Materials*, edited by Rudy J. M. Konings (Elsevier, Oxford, 2012), pp. 1–31.
[35] T. Bullough and J. R. Willis, Philos. Mag. **31**, 855 (1975).
[36] P. T. Heald and M. V. Speight, Acta Metall. **23**, 1389 (1975).
[37] F. R. N. Nabarro, R. Bullough, and J. R. Matthews, Acta Metall. **30**, 1761 (1982).
[38] C. H. Woo, J. Nucl. Mater. **120**, 55 (1984).
[39] G. Carpenter, R. Zee, and A. Rogerson, J. Nucl. Mater. **159**, 86 (1988).
[40] V. Fidleris, J. Nucl. Mater. **159**, 22 (1988).
[41] H. Rouchette, L. Thuinet, A. Legris, A. Ambard, and C. Domain, Phys. Rev. B **90**, 014104 (2014).
[42] G. Vérité, C. Domain, C.-C. Fu, P. Gasca, A. Legris, and F. Willaime, Phys. Rev. B **87**, 134108 (2013).
[43] G. D. Samolyuk, S. I. Golubov, Y. N. Osetsky, and R. Stoller, Philos. Mag. Lett. **93**, 93 (2013).
[44] M. I. Mendelev and G. J. Ackland, Philos. Mag. Lett. **87**, 349 (2007).
[45] F. Willaime and C. Massobrio, Phys. Rev. B **43**, 11653 (1991).
[46] C. Varvenne, O. Mackain, L. Proville, and E. Clouet, Acta Mater. **102**, 56 (2016).
[47] N. de Diego, A. Serra, D. J. Bacon, and Y. N. Osetsky, Modell. Simul. Mater. Sci. Eng. **19**, 035003 (2011).
[48] O. H. Nielsen and R. M. Martin, Phys. Rev. B **32**, 3780 (1985).
[49] A. K. Subramaniyan and C. Sun, Int. J. Solids Struct. **45**, 4340 (2008).
[50] W. Cai, V. V. Bulatov, J. Chang, J. Li, and S. Yip, Philos. Mag. **83**, 539 (2003).
[51] J. D. Eshelby, Proc. R. Soc. London A **241**, 376 (1957).
[52] T. Albaret, A. Tanguy, F. Boioli, and D. Rodney, Phys. Rev. E **93**, 053002 (2016).
[53] P. Narang, G. Paul, and K. Taylor, J. Less-Common Met. **56**, 125 (1977).
[54] R. Khoda-Bakhsh and D. K. Ross, J. Phys. F: Met. Phys. **12**, 15 (1982).
[55] P. Giannozzi, S. Baroni, N. Bonini, M. Calandra, R. Car, C. Cavazzoni, D. Ceresoli, G. L. Chiarotti, M. Cococcioni, I. Dabo, *et al.*, J. Phys.: Condens. Matter **21**, 395502 (2009).
[56] J. P. Perdew, K. Burke, and M. Ernzerhof, Phys. Rev. Lett. **77**, 3865 (1996).
[57] E. Clouet, Phys. Rev. B **86**, 144104 (2012).
[58] C. Varvenne, O. Mackain, and E. Clouet, Acta Mater. **78**, 65 (2014).
[59] M. P. Puls and C. H. Woo, J. Nucl. Mater. **139**, 48 (1986).
[60] H. R. Schober, J. Nucl. Mater. **126**, 220 (1984).
[61] P. Dederichs, C. Lehmann, H. Schober, A. Scholz, and R. Zeller, J. Nucl. Mater. **69–70**, 176 (1978).
[62] B. Puchala, M. L. Falk, and K. Garikipati, Phys. Rev. B **77**, 174116 (2008).
[63] S. MacEwen, C. Coleman, C. Ells, and J. Faber, Acta Metall. **33**, 753 (1985).
[64] E. S. Fisher and C. J. Renken, Phys. Rev. **135**, A482 (1964).
[65] J. Goldak, L. T. Lloyd, and C. S. Barrett, Phys. Rev. **144**, 478 (1966).
[66] M. Christensen, W. Wolf, C. Freeman, E. Wimmer, R. B. Adamson, L. Hallstadius, P. E. Cantonwine, and E. V. Mader, J. Phys.: Condens. Matter **27**, 025402 (2015).
[67] E. Kröner, in *Theory of Crystal Defects*, edited by F. Kroupa (Academia, 1964), pp. 215–230.